LAWRENCE
LIVERMORE
NATIONAL
LABORATORY

LLNL-JRNL-657799

Evolution of Helical Perturbations in a Thin-Shell Model of an Imploding Liner

D. D. Ryutov

July 28, 2014

The Physics of Plasmas

Disclaimer

LLNL-JRNL-657799

EVOLUTION OF HELICAL PERTURBATIONS IN A THIN-SHELL MODEL OF AN IMPLODING LINER

D.D. Ryutov
Lawrence Livermore National Laboratory, Livermore, CA 94550, USA

Abstract

A thin-shell model of the liner stability has been revisited and applied to the stability of the helical perturbations. Several stages of the implosion have been identified, starting from a long initial "latent" phase of an almost resting liner, continuing to the second stage of a rapid contraction and significant perturbation growth, and then transitioning to the third stage where perturbations become ballistic and highly non-linear. The stage of stagnation and rebound is beyond the scope of this paper. An importance of vorticity conservation during the late stages is emphasized. Nonlinear evolution of perturbations is followed up to the point of the formation of cusp structures. Effects of in-surface flows and of their enhancement due to the vorticity conservation are discussed. It is shown that the pre-machined perturbations created only on the outer surface of the liner grow much slower than one could anticipate. The limitations on the thin-shell description are discussed.

I. INTRODUCTION

The physics of magnetically imploded conducting shells is an interesting problem of non-linear magneto-hydrodynamics (MHD) and has drawn significant attention in the past. In addition to its fundamental importance (see, e.g., original papers [1-4] and reviews [5, 6]) it has also a number of applications, especially in fusion research, e.g. [7-9] and in radiation generation, e.g. [10, 11]. Imploding shells can also serve as a platform for the studies in the area of laboratory astrophysics, e.g. [12, 13].

We consider implosion of an empty cylindrical shell driven by a magnetic pressure of the azimuthal field (the Z-pinch geometry) or, in some cases, by a combination of the azimuthal and axial fields (the screw-pinch geometry). The thin-shell model is based on the assumption that the shell thickness is less than all other important parameters of the dimension of length: pinch radius and length, and both azimuthal and axial wavelength of the perturbations. At the same time, the shell is considered as perfectly conducting, so that the drive field does not penetrate through the shell. This set of constraints may not necessarily hold through the whole implosion process of a real liner and therefore would not allow us to reach a consistent description of the whole process. On the other hand, this model can provide important insights into the physics of specific individual effects and help in developing an intuitive explanation for some of them.

We include in the analysis the helical modes with the finite azimuthal mode number m. We focus on the linear stability, although a qualitative discussion of some non-linear effects is also provided. As mentioned, the model of a thin shell is based on the assumption that the liner thickness h is small compared both to the wavelength of the perturbations and the instantaneous shell radius $a(t)$. Under such conditions, the internal

structure of the shell becomes unimportant and the shell is characterized by a single parameter, μ, the mass per unit surface area [1, 2].

A linear stability analysis of a thin cylindrical shell imploded by the magnetic pressure was performed in a seminal paper by E.G. Harris [1]. E.G. Harris has considered the situations where the drive field is directed either azimuthally (as in the Z-pinch) or axially (as in the theta pinch) and derived expression for the instantaneous growth rate. To describe the helical perturbations in the case of a screw-pinch drive we have to include both azimuthal and axial fields simultaneously and we do that below. We extend our linear analysis beyond the model of the instantaneous growth rate in Sec. IV and V. Another difference of our paper from Ref. 1 is in the proper accounting for the azimuthal momentum evolution of the imploding shell. We discuss this latter issue in Sec. II and VI.

An elegant analysis by T. Ott [2] addressed instability of a thin planar shell driven by a light (formally massless) gas; it was shown that, by using Lagrangian description, one can obtain a complete non-linear solution for an x-y flow. This analysis was later generalized to the "flute" perturbation of a cylindrical shell driven by the pressure of an axial field [3]. Another extension of Ott's analysis was a study of non-linear evolution of an axisymmetric perturbation of a thin shell driven by a massless gas [4]. Note that the magnetic drive, generally speaking, cannot be reduced to the massless gas drive considered in Refs. 2, 4, as in this case there is no pressure perturbation on the liner surface, whereas in the case of a magnetic drive, generally speaking, the pressure is perturbed (except for some special cases, like the case of flute perturbations driven by a purely axial field as in Ref. 3).

Other aspects of the helical perturbations of the Z-pinch have been studied for the equilibrium situations (no acceleration/deceleration of the liner surface), see the classical analyses by Kruskal and Shafranov [14, 15] and an excellent summary in a review by Kadomtsev [16]. The instability of an equilibrium pinch is related to the unfavorable curvature of the magnetic field at the pinch surface. In more recent history, a lot of attention was directed also to the effect of the line-tying at the ends of the equilibrium pinch (e.g., [17-20]). Unlike the references [14-20], we consider here instability of an *accelerated* shell, where the equivalent gravity force has a significant and even decisive dynamical effect, making the instability to look like a Rayleigh-Taylor instability, whence the sometimes used term "Magneto-Rayleigh-Taylor" (MRT) instability. In this paper, following the analysis by E.G. Harris, we account for both types of the instability drive: acceleration and unfavorable field curvature.

Recently, the studies of helical perturbations have acquired additional significance in conjunction with their experimental identification in the pioneering experiments by researchers from Sandia National Laboratories [21, 22]. The present paper does not pretend to provide a complete self-consistent picture of a very complex dynamical system but it may help in developing physical intuition. The author describes and analyses several stages of the implosion and attempts to identify most salient features of each stage. The connection between the stages is made on a qualitative level. The very late stage of the implosion, where the plasma inside the liner becomes so dense and hot that its pressure begins to affect the liner dynamics is not considered at all. Still, with these limitations a more or less complete picture of a thin-shell implosion emerges, from the cold start, to the end of the run-in phase, where the liners transitions to the stagnation phase (not covered here).

II. BASIC EQUATIONS

A. The geometry and the drive field

In the unperturbed state, the shell is assumed to be an axisymmetric imploding cylinder. The magnetic field that compresses it may have two components: an azimuthal field B_φ of an axial current (as in the Z-pinches) and an axial field B_z (as in the theta-pinches), giving rise to the screw-pinch geometry. The plasma pressure outside the liner is assumed to be negligibly small, so that the liner acceleration is entirely determined by the magnetic pressure acting on its surface. We neglect the presence of an axial field and plasma inside the liner: their pressure is small compared to the drive pressure until very late stage of the implosion. In principle, one can include them into the thin-shell model, but this would make the analysis too lengthy. We assume that the radius of the return current conductor is much greater than the initial liner radius and the pinch length is much greater than the wavelength of the perturbations, so that the edge effects are unimportant.

One can consider various time-histories of the azimuthal and axial driving fields. To make the study manageable, we assume that the axial field constitutes some constant fraction of the azimuthal field:

$$B_z(t) = \alpha B_\varphi(t) \tag{1}$$

Although our general results cover arbitrary values of α, we focus on the situations where the axial field is dominant, so that α is small.

B. Unperturbed motion

Thin-shell model provides a good description for the modes with modest axial wave number k and azimuthal mode number m. Specifically, its applicability is constrained by the conditions

$$kh<1,\ mh/a<1, \tag{2}$$

where h is the shell thickness. A great advantage of this model is related to its ability to describe the features of the helical perturbations by simple analytical tools.

Unperturbed motion of the shell is a radial implosion, where the position of the shell $a(t)$ is described by the equations

$$\mu(t)\frac{d^2a}{dt^2} = -p(t)\ , \tag{3}$$

$$\frac{d}{dt}\left[a(t)\mu(t)\right] = 0\ , \tag{4}$$

where $p(t)$ is the magnetic pressure and μ is the mass per unit surface area. Equation (4) is a mass conservation equation for the cylindrical shell. Equations (3)-(4) correspond to the unperturbed axisymmetric implosion, prior to the imposition of small perturbations. A convenient characteristic of the implosion process is an absolute value of the instantaneous acceleration,

$$g(t) = \frac{p(t)}{\mu(t)}\ . \tag{5}$$

Note that g is positive in our analysis (i.e., the sign convention is different from Ref. 1). The unperturbed magnetic field has an axial component B_z and an azimuthal component B_φ, and the unperturbed pressure is

$$p = \frac{B_\varphi^2 + B_z^2}{8\pi} = \left(1+\alpha^2\right)\frac{B_\varphi^2}{8\pi} \tag{6}$$

where the fields are evaluated at the liner surface. The driving pressure in this model scales as B_φ^2 or as I^2/a^2, where I is a Z-pinch current.

A salient feature of the liner implosions is the presence of a long "latent phase" when the current gradually rises to high values, but the liner does not yet move by any significant distance, so that $\Delta a \equiv a_0 - a(t) << a_0$. This feature is a result of the structure of the governing equation (3): the liner displacement is a result of two integrations over the time, so that it remains small even after the acceleration g and growth rates have already reached significant values. A nice example of the exact solution of Eq. (3) for the bell-shaped current profile is presented in Slutz et al. [23].

A reasonable approximation for the current at an early stage of the implosion is a linear function of time, this yielding a parabolic dependence of $g(t)$ at this stage:

$$g(t) = g_0\left(\frac{t}{\tau}\right)^2 . \tag{7}$$

For the parabolic model (7), the shell radius changes as

$$a = a_0\left[1 - \frac{g_0\tau^2}{12a_0}\left(\frac{t}{\tau}\right)^4\right]. \tag{8}$$

We set then g_0 to be

$$g_0 = \frac{2a_0}{\tau^2} . \tag{9}$$

This choice of parameters fits quite well the Slutz's et al. analytical model [23] until $t=\tau$, if τ is chosen to be 0.8 of the total implosion time. As Eq. (8) shows, the change of the radius at $t=\tau$ is indeed about 15% of the initial radius, so that the model of a constant radius is well justified up to $t=\tau$. The liner velocity at $t=\tau$ is:

$$\mathrm{v}_0 = \frac{g_0\tau}{3} = \frac{2}{3}\frac{a_0}{\tau} . \tag{10}$$

At later stages, the radius starts changing very rapidly and an approximation of the constant radius breaks down.

An interesting feature of the implosion is that, starting from $t=\tau$, the current changes only by ~10% with respect to its value at the end of the latent phase (see, e.g., Refs. 5, 7, 22). In other words, the current at the final stage of the implosion can be approximately considered as a constant. Equations (3)-(4) are then reduced to:

$$\frac{d^2a}{dt^2} = -\frac{const}{a} = -g_0\frac{a_0}{a} = -2\frac{a_0^2}{a\tau^2} . \tag{11}$$

The subsequent evolution of the liner velocity can be found from the first integral of Eq. (11):

$$\dot{a} = -\mathrm{v}_0\sqrt{1 + 9\ln\frac{a_0}{a}} . \tag{12}$$

Interestingly, the velocity changes by a relatively small amount at the late stage (but still before the deceleration begins): for example, between the radial convergence of 10 and a radial convergence of 20, the velocity changes by a mere 10%.

One can introduce a characteristic time t^* for the change of the pinch radius:

$$t^* \equiv \frac{a}{|\dot{a}|} . \tag{13}$$

As seen from Eqs. (12)-(13), at the late stage, t^* decreases approximately as a towards the liner collapse. We will use this circumstance in Sec. III.

C. Linearization

In the linear regime the evolution of the shell can be described by the displacements of the material elements of the shell in the radial (r), azimuthal (φ) and axial (z) directions, with respect to the positions of these elements on the unperturbed radially imploding shell (Fig. 1). We denote the radial and axial displacements as $\xi_r(\varphi,z,t)$ and $\xi_z(\varphi,z,t)$, respectively. For the azimuthal displacement it is convenient to characterize it by the change $\delta\varphi(\varphi,z,t)$ of the azimuthal angle of the material element. We emphasize that those are displacements with respect to the instantaneous position of the fluid element on the unperturbed (but moving) shell. With these variables, the continuity equation is:

$$\delta\mu + \mu\left(\frac{\partial\delta\varphi}{\partial\varphi} + \frac{\partial\xi_z}{\partial z}\right) = 0 . \tag{14}$$

Three components of the momentum equation read as:

$$\frac{\partial^2\xi_r}{\partial t^2} = g\left(\frac{\delta\mu}{\mu} - \frac{\delta p}{p}\right) \tag{15}$$

$$\frac{\partial}{\partial t}\left(a^2\frac{\partial\delta\varphi}{\partial t}\right) = g\frac{\partial\xi_r}{\partial\varphi} \tag{16}$$

$$\frac{\partial^2\xi_z}{\partial t^2} = g\frac{\partial\xi_r}{\partial z} \tag{17}$$

As ξ_r is a displacement along the radial coordinate directed outward, the positive ξ_r corresponds to the element lagging behind the imploding shell (Fig. 1).

The magnetic pressure perturbation has to be found by solving the electromagnetic equations outside the liner. [This calculation can be found, e.g., in Ref. 1; in order to have it readily available to the reader, we present its brief summary in Appendix A.] Note the difference between Eq. (16) and the corresponding Eq. (51) in Ref. 1: in the latter, the change of the shell radius does not cause the change of the azimuthal velocity, whereas our Eq. (16) accounts for this effect (which, in the absence of external forces, is simply azimuthal momentum conservation). [Note a typo in Eq. (51) of Ref. 1: there should be ξ_φ, not ξ_r on the left-hand side. There are also typos in Eq. (40) where ξ_φ should be replaced by ξ_r and $\partial\xi_r/\partial r$ by $\partial\xi_r/\partial z$.] The rest of equations, up to notation, are the same as in Ref. 1. The aforementioned subtle change of Eq. (16) does not affect the evaluation of the instantaneous growth rate, i.e., it does not affect the main

result of Ref. 1. It affects however the amplitude of perturbations in the imploding liner. We dwell on that aspect in Sec. V.

D. Vorticity and energy

From Equations (16) and (17) it follows the conservation of vorticity of the surface flow:

$$a^2 \frac{\partial \delta\dot{\varphi}}{\partial z} - \frac{\partial \delta\dot{\xi}_z}{\partial \varphi} \equiv V = const\,, \tag{18}$$

where dots indicate time derivatives.

The kinetic energy of the perturbation per unit length along the axis is:

$$\pi\mu r \left\langle \left[\dot{\xi}_r^2 + \left(r\delta\dot{\varphi}\right)^2 + \dot{\xi}_z^2 \right] \right\rangle_{\varphi} \tag{19}$$

where $\dot{\xi}_r \equiv \partial \xi_r / \partial t$, and the same for the other components. Taking the time derivative and noting that, according to Eq. (3), $\mu a = const$, we find:

$$\frac{1}{2}\frac{d}{dt}\left\langle \left[\dot{\xi}_r^2 + \left(r\delta\dot{\varphi}\right)^2 + \dot{\xi}_z^2 \right] \right\rangle_{\varphi,z} =$$
$$g\left\langle \left[\left(\frac{\delta\mu}{\mu} - \frac{\delta p}{p} \right)\dot{\xi}_r + \left(-r\dot{r}\delta\dot{\varphi}^2 + \delta\dot{\varphi}\frac{\partial \xi_r}{\partial \varphi} \right) + \dot{\xi}_z \frac{\partial \xi_r}{\partial z} \right] \right\rangle_{\varphi,z} . \tag{20}$$

E. Harmonic perturbations

As the unperturbed system is axisymmetric and translationally-symmetric, one can seek perturbations of the form $f(t)\exp(ikz - im\varphi)$. For such a perturbation one has:

$$\delta\mu = -i\mu\left(-m\delta\varphi + k\xi_z\right), \tag{21}$$

$$\frac{\partial}{\partial t}\left(a^2 \frac{\partial \delta\varphi}{\partial t} \right) = -img\xi_r\,, \tag{22}$$

$$\frac{\partial^2 \xi_z}{\partial t^2} = ikg\xi_r\,, \tag{23}$$

The set of equations (15) and (21)-(23) describes the stability of a thin liner with the effect of a radial convergence included. The most obvious effect of radial convergence is a growth of the azimuthal velocity, Eq. (22).

In a number of cases, it may be more convenient to seek the solution in a real form. We will use the representation $f_p(t)\cos(kz - m\varphi)$ where f_p is a time-dependent amplitude with a subscript "p" indicating that this is an amplitude of the pressure perturbation. An inspection of the set (15), (21)-(23) shows that perturbations of the other quantities will then have a sine or cosine form, with

$$\delta\mu = f_\mu \cos(kz - m\varphi)\,,\ \xi_r = f_r \cos(kz - m\varphi)\,, \tag{24}$$

$$\delta\varphi = f_\varphi \sin(kz - m\varphi)\,,\ \xi_z = f_z \sin(kz - m\varphi)\,, \tag{25}$$

with the time-dependent amplitudes being related by

$$f_\mu = -\mu\left(-mf_\varphi + kf_z\right), \tag{26}$$

$$\frac{d^2 f_r}{dt^2} = g\left(\frac{f_\mu}{\mu} - \frac{f_p}{p}\right), \tag{27}$$

$$\frac{d}{dt}\left(a^2 \frac{df_\varphi}{dt}\right) = mgf_r, \tag{28}$$

$$\frac{d^2 f_z}{dt^2} = -kgf_r. \tag{29}$$

The magnetic pressure perturbation can be expressed in terms of deviation of the liner shape from a cylinder, i.e., in terms of the function $\xi_r(\varphi, z)$. For the harmonic perturbations it has a form

$$\delta p / p = Q(m,k,t) f_r. \tag{30}$$

The function $Q(m,k,t)$ is derived in Ref. 1 and summarized in Appendix B and is:

$$Q = \frac{2}{\left(B_\varphi^2 + B_z^2\right)ka^2}\left[\left|\frac{K_m}{K_m'}\right|\left(mB_\varphi - kaB_z\right)^2 - kaB_\varphi^2\right], \tag{31}$$

where $K_m(ka)$ is a modified Bessel function. The derivative K_m' is taken over the whole argument. This derivative is negative at all values of the argument. To emphasize that the first term in the square brackets is positive (stabilizing) we have written $|K_m / K_m'|$ instead of $-K_m / K_m'$. We also remind that the wave number k is assumed to be positive, whereas m can be of either sign, determining the handedness of the perturbations..

For the axisymmetric perturbations, m=0, one has:

$$\left|\frac{K_0}{K_0'}\right| \approx ka\ln\left(\frac{1}{ka}\right), \quad ka << 1; \quad \left|\frac{K_0}{K_0'}\right| \approx 1, \quad ka >> 1. \tag{32}$$

For $|m| \geq 1$, ka>1 one has:

$$\left|\frac{K_m}{K_m'}\right| \approx \frac{ka}{\sqrt{m^2 + k^2 a^2}} \tag{33}$$

The function Q vs ka for several values of B_z / B_φ is presented in Fig. 2.

The stability problem has been reduced to the set of ordinary differential equations (27)-(29) that covers, in particular, a possibility of the time-varying pressure drive and acceleration. In a sometimes considered reference problem, where the piston is driven by a pressure of a massless gas (as in Refs. 2, 4), one has simply f_p=0. In Eq. (27)

As the system is described by three second-order differential equations (27)-(29), a complete set of the initial conditions should contain initial values of six quantities, f_r, f_φ and f_z and their first time derivatives. Solution for the set (27)-(29) would then characterize the evolution of the initial perturbation until it reaches a well-developed state, where the fastest-growing mode becomes strongly dominant.

III. QUALITATIVE CHARACTERIZATION OF THE INSTABILITY REGIMES

The instability in the system with the varying parameters is often characterized by the instantaneous growth rate Γ. In our case, this instantaneous growth rate can be evaluated by "freezing" all the varying parameters (like a) at their instantaneous values

and then seeking for the solution evolving as $\exp(\Gamma t)$. The set of equations (26)-(29) yields the following equation for Γ:

$$D(\Gamma,t) \equiv \Gamma^4 + gQ\Gamma^2 - \frac{g^2}{a^2}\left(m^2 + k^2a^2\right) = 0 . \tag{34}$$

The solution to this equation is:

$$\Gamma_{1,2}^2 = \frac{g}{2}\left[-Q \pm \sqrt{Q^2 + 4(k^2 + m^2/a^2)}\right] \tag{35}$$

For the subscript of "1" one of the two roots corresponds to exponential growth and the other to exponential decay; for the subscript "2" there are two oscillatory roots (analogs of sine and cosine solutions).

A rough estimate of the instantaneous growth rate is

$$\Gamma \sim \sqrt{qg} , \tag{36}$$

where

$$q = \sqrt{k^2 + \frac{m^2}{a^2}} . \tag{37}$$

One has, however, to remember that the concept of instantaneous growth rate can be used only if the change of the growth rate during one e-folding time $1/\Gamma$ is smaller than the growth rate itself, i.e., only if the condition

$$\frac{1}{\Gamma}\left|\frac{d\Gamma}{dt}\right| << \Gamma \tag{38}$$

holds. This regime can also be characterized by the dimensionless parameter ε:

$$\varepsilon = \frac{1}{\Gamma^2}\left|\frac{d\Gamma}{dt}\right| << 1 . \tag{39}$$

Condition (38) is certainly not satisfied at an early stage of the implosion, where g varies as t^2: the left-hand side of Eq. (38) scales then as $1/t$, whereas the right-hand side scales as t. Therefore, the perturbation growth at an early stage cannot be characterized by the concept of an instantaneous growth rate and has to be described by a complete set of Eqs. (26)-(29) with a=const but g varying in time. A solution of this problem is presented in Sec. IV.

For higher wave-numbers q, condition (38) may be fulfilled at the later part of the latent phase, whereas for lower wave-numbers it may be reached at the stage where the acceleration begins to increase due to the decrease of a. This second stage, where the condition (38) is satisfied, can be described by the WKB (Wentzel-Kramers-Brillouin) approach (see, e.g. Ref. 24), which yields not only the exponentiation factor, $E_0 = \int \Gamma\, dt$, but also a pre-exponential multiplier which can be quite important for the converging liner: knowing this factor, one can match the WKB solution to the solution for the "latent" stage and thereby directly relate the WKB solution to the initial perturbations. This WKB analysis is presented in Sec. V.

Surprisingly, for some range of the wave numbers the acceleration (g) drive of the MRT instability may again become small. Indeed, according to Eqs. (13) and (36), condition (38) may break down again for small a, now due to the shortened ($\sim a$) implosion time-scale t^*, Eq. (13). In other words, the effect of the liner acceleration, g, at this (third) stage of the implosion becomes unimportant. This does not mean that the

perturbations do not grow: they continue to evolve ballistically, with the acceleration of each fluid element being negligible. As the liner radius is already relatively small, this "ballistic" deformation can be very significant. This stage of the implosion is described in Sec. VI.

Finally, if the shell had not lost its integrity at the previous three stages, a reaction of the compressed fuel and magnetic field inside the liner become dominant over the external compression force, and the liner decelerates and rebounds. The transition to this fourth stage occurs very near the point of the maximum compression: it suffices to say that the magnetic pressure inside the liner grows as $1/a^4$, so that the change of the radius from 1.5 of the minimum value to the minimum value leads to the increase of the pressure by a factor of 5. We do not attempt to cover this final stage by our analysis, as it would require a description of the plasma and magnetic field in a non-trivial setting, which constitutes a big project of its own. We direct the reader to the papers [7-9] where this state was considered, and Ref. [25] where the back reaction of a plasma with embedded magnetic field on the liner stability was assessed in the simple planar geometry.

IV. AN EARLY STAGE OF THE INSTABILITY

A. Equations with *a*=const

A salient feature of the liner implosions is the presence of a long "latent phase" when the current gradually rises to high values, but the liner does not yet move by any significant distance, so that $\Delta a \equiv a_0 - a(t) << 1$. This feature is a result of the structure of the governing equation (3): the displacement is a result of two integrations over the time, so that it remains small even after the acceleration and growth rates have already reached high values. A nice example of the exact solution of Eq. (3) for the bell-shaped current profile is presented in Ref. 23.

This latent phase is the one where the axial magnetic field may still be dynamically-significant compared to the azimuthal field. The exponentiation factor of the perturbations at this stage determines the "initial state" for the instability at the later stages, after the liner eventually "takes off" and rapidly implodes.

At this initial stage (which, as we have mentioned in Sec. IIA, occupies ~ 70-80 % of the total duration of the liner implosion, see Refs. 7 and 23, the radius of the shell in Eq. (28) can be considered as a constant. An unperturbed areal mass density μ is also constant. This allows one to reduce the set of equations (26)-(29) to:

$$f_\mu = -\mu_0 \left(-m f_\varphi + k f_z \right), \tag{40}$$

$$\ddot{f}_r = -g \left[-m f_\varphi + k f_z + Q f_r \right], \tag{41}$$

$$\ddot{f}_\varphi = \left(m / a_0^2 \right) g f_r, \tag{42}$$

$$\ddot{f}_z = -g k f_r, \tag{43}$$

with a_0 being the initial shell radius and μ_0 being the initial surface mass density. Note that the right-hand side of these equations depends explicitly on time, via the function $g(t)$ that changes as I^2. The coefficient Q does not depend on time provided B_z is proportional

to B_φ. Otherwise, Q may also depend on time. As before, the solution is uniquely determined by the initial values of the variables f_r, f_φ and f_z and their derivatives.

By some simple manipulations, one can eliminate f_φ and f_z and reduce this set of equations to two coupled second-order equations for f_r and f_m:

$$\ddot{f}_r = g\left[\frac{f_\mu}{\mu_0} - Qf_r\right] \tag{44}$$

$$\frac{\ddot{f}_\mu}{\mu_0} = g\left(\frac{m^2}{a_0^2} + k^2\right) f_r, \tag{45}$$

plus one separate equation for the quantity $U \equiv ka_0^2 f_\varphi + mf_z$:

$$\ddot{U} = 0 \tag{46}$$

related to vorticity, Eq. (18), by $\dot{U} = V$.

The set of three second-order differential equations (44)-(46) allows one to find a solution in terms of the initial values of the variables f_r, f_μ and U, and their first derivatives. Note that these variables are uniquely related to the variables f_r, f_φ and f_z, so that the solution of the set (44)-(46) immediately yields the solution of the set (40)-(43). Initially, the solution is certainly non-WKB; however, later in the pulse, for t approaching τ (but a being still almost constant) the solution may enter the WKB regime. This allows one to relate the amplitude of the amplitude of the WKB solution to the initial (t=0) perturbations by matching the solutions in the overlap domain.

B. Solution of the initial value problem

We consider in some detail the solution of the set (44)-(46) for the case where the parameter Q is constant, whereas the acceleration g may vary with time. This model corresponds to the situation where the axial field near the surface varies in concert wth the azimuthal field, $B_z(t) = \alpha B_\varphi(t)$, with α=const. The acceleration g at this stage scales as a square of the driving current.

We will show below that the set of equations (44)-(46) allows one to obtain a general description of the instability for arbitrary initial conditions and arbitrary function *g(t)*. Let us look for the solution of the form

$$f_r = \kappa \frac{f_\mu}{\mu_0} \tag{47}$$

where κ is some constant independent of time that will be found shortly. Substituting it to equations (44)-(45), one finds the following algebraic equation for the eigenvalues of κ:

$$\left(\frac{m^2}{a_0^2} + k^2\right)\kappa^2 + Q\kappa - 1 = 0 \tag{48}$$

There are two solutions to this equation, directly related to the formally defined instantaneous growth rate (35):

$$\kappa_{1,2} = \frac{\Gamma_{1,2}^2}{g\left(k^2 + m^2 / a_0^2\right)} \ . \tag{49}$$

Remarkably, $\kappa_{1,2}$ do not depend on time, although g does. For each of them the system (44)-(46) is reduced to a single second-order equation,

$$\ddot{f}_r = g\left(\frac{m^2}{a_0^2} + k^2\right)\kappa f_r \tag{50}$$

with f_μ related to f_r by Eq. (40). For the positive sign of κ, i.e., for $\kappa = \kappa_1$, Eq. (50) has two solutions, an exponentially growing and an exponentially decaying ones. For $\kappa < 0$, i.e., for $\kappa = \kappa_2$, there are two oscillatory solutions analogous to sine and cosine solutions.

We will designate these solutions as Y_1 and Z_1 for $\kappa = \kappa_1$ and Y_2 and Z_2 for $\kappa = \kappa_2$. We then arrive at the following general solution of the problem:

$$\begin{aligned} &f_r = AY_1 + BZ_1 + CY_2 + DZ_2; \\ &\kappa_1\kappa_2 f_\mu / \mu_0 = \kappa_2\left(AY_1 + BZ_1\right) + \kappa_1\left(CY_2 + DZ_2\right) \end{aligned} \tag{51}$$

where A-D are arbitrary constants. For the initial value problem, where the values of f_r, f_μ and $\dot{f}_r, \dot{f}_\mu$ at t=0 are specified, these constants are determined from the set of four linear equations for A-D.

For the problem under consideration, it is convenient to choose a specific set of the basis functions. For the solutions corresponding to κ=κ_1, we choose the exponentially-growing solution with a zero derivative at t=0; we choose an arbitrary multiplier so as to make the solution equal to 1 at t=0. For exponentially decaying solution we choose the multiplier so as to make this solution also equal to 1 at t=0. So, we have

$$Y_1(0) = 1; \ \ \dot{Y}_1(0) = 0; \ \ Z_1(0) = 1 \tag{52}$$

For the oscillating solutions corresponding to κ=κ_2, we choose one of them to be equal to 1 and have a zero derivative at t=0; for the second solution we choose the one that is zero at t=0. We adjust the coefficient in such a way as to make the derivative of this solution to be equal to the derivative of Z_1, In other words, the second set of eigenfunctions has the properties:

$$Y_2(0) = 1; \ \ \dot{Y}_2(0) = 0; \ \ Z_2(0) = 0; \ \ \dot{Z}_2(0) = \dot{Z}_1(0) \tag{53}$$

An example of the eigenfunctions for the parabolic temporal dependence of the acceleration is presented in Appendix B.

The choice (52), (53) of the eigenfunctions allows one to write a convenient solution of the initial value problem in a remarkably symmetric form, in which there is a separation of the contributions of the initial displacements and velocities. Indeed, from Eqs. (51), we find:

$$A = \frac{\kappa_1 f_{r0} - \kappa_1\kappa_2 \dfrac{f_{\mu 0}}{\mu_0}}{\kappa_1 - \kappa_2}; \ \ C = -\frac{\kappa_2 f_{r0} - \kappa_1\kappa_2 \dfrac{f_{\mu 0}}{\mu_0}}{\kappa_1 - \kappa_2} \ , \tag{54}$$

$$B = \frac{\kappa_1 \dot{f}_{r0} - \kappa_1\kappa_2 \dfrac{\dot{f}_{\mu 0}}{\mu_0}}{\left(\kappa_1 - \kappa_2\right)\dot{Z}_1(0)}; \ \ D = -\frac{\kappa_2 \dot{f}_{r0} - \kappa_1\kappa_2 \dfrac{\dot{f}_{\mu 0}}{\mu_0}}{\left(\kappa_1 - \kappa_2\right)\dot{Z}_1(0)} \ . \tag{55}$$

The most common (and, perhaps, relevant) formulation of the initial value ptoblem is the one where at t=0 there exist some static perturbations, i.e., initial values of f_r and f_μ are non-zero, while their time derivatives are zero. Then one has to set B=D=0, whereas the other two constants, A and C, are related to the initial values by Eq. (54).

Depending on the initial values of f_r and f_μ there may be some period when the surface oscillates, before the exponentially growing mode takes over. There is also a special type of perturbations where $\kappa_2 f_{\mu 0} = \mu_0 f_{r0}$, for which the mode of exponential growth does not show up. If this condition is not satisfied (as is usually a case), then the exponentially growing solution becomes dominant, and f_r and f_μ follow Eqs. (51) where only terms proportional to Y_1 have to be retained.

Now we turn to Eq. (46). It shows that the quantity $\dot{U} = \dot{f}_z + \frac{ka_0}{m} a_0 \dot{f}_\varphi$ is constant in time. This quantity is the velocity component along the line of a constant phase and describes a vortex part of the velocity field, the one that does not perturb the density. This component is uncoupled from the other equations and does not affect the development of the instability. Without loss of generality, one can therefore assume that both $\dot{U}$ and U are simply zero. In other words, we can limit ourselves to considering only perturbations for which

$$f_\varphi = -m f_z / k a_0^2 \tag{56}$$

On the other hand, Eq. (40) shows that

$$m f_\varphi - k f_z = \frac{f_\mu(t)}{\mu_0}, \tag{57}$$

where $f_\mu(t)$ is a known function of time, Eq. (51). Accordingly, Eqs. (56) and (57) define the temporal dependence of the two other components of the displacement vector:

$$f_\varphi(t) = \frac{m f_\mu(t) / \mu_0}{m^2 + k^2 a_0^2} \tag{58}$$

$$f_z(t) = -\frac{k a_0^2 f_\mu(t) / \mu_0}{m^2 + k^2 a_0^2} \tag{59}$$

C. Relation to machined perturbations

In the experiments on liner stability, the perturbations are usually machined by removing material from the liner surface. In a thin-shell model this means the presence of a correlation between components f_r and f_μ of initial perturbations. Consider for example perturbation machined to the outer surface of a liner, Fig. 3. The average unperturbed surface would be situated at the distance $\zeta/2$ from the initial surface. The surface density variation will then be

$$f_{\mu 0} = \frac{\mu_0}{2h} \zeta . \tag{60}$$

The amplitude of the radial displacement of a liner will be $f_{r0} = \zeta/4$. In other words, the initial surface mass density perturbation and initial waviness of the liner will be related to each other:

$$f_{r0} = \frac{h}{2}\frac{f_{\mu 0}}{\mu_0} \tag{61}$$

We neglect here a second-order correction related to the change of the average thickness caused by the removal of some material.

What is remarkable here is that Eq. (61) that relates f_{r0} to $f_{\mu 0}$ contains the shell thickness *h*, which is assumed to be small both compared to the shell radius a and an inverse wave number k^{-1}. When one substitutes this result into Eq. (54), one sees that the initial perturbation of μ strongly dominates the effect of initial rippling, by a factor of roughly *1/kh*. This basically means that the subsequent evolution of the perturbations is almost entirely caused by the initial mass density perturbation.

In the spirit of a thin-shell model, one can attribute the initial surface mass-density perturbation to the initial displacement of the material in the *z* and φ directions, by Eqs. (58) and (59). Note that this discussion relates to pre-machined perturbations with any *m* and *k* satisfying the thin-shell model, $k<1/h$, $m/a<1/h$.

If one neglects the initial f_r in Eqs. (46), the following solution emerge3:

$$\begin{aligned} f_r &= -\frac{\kappa_1\kappa_2}{\kappa_1-\kappa_2}\frac{f_{\mu 0}}{\mu_0}\left(Y_1 - Y_2\right); \\ f_\mu &= f_{\mu 0}\frac{\left(-\kappa_2 Y_1 + \kappa_1 Y_2\right)}{\kappa_1-\kappa_2}, \end{aligned} \tag{62}$$

with $f_{\mu 0}$ related to the initial depth ζ of the machined material (Fig. 4) by Eq. (53). Specific examples are presented in the next section.

For a developed instability the first, exponentially growing terms in Eq. (47) become dominant. This leads to a simple relation between f_r and f_μ at this stage:

$$f_r = \kappa_1 f_\mu / \mu_0 \tag{63}$$

At this developed stage, the perturbation of the shape of the shell would look as shown in Fig. 4, with the ripples at the outer side of the liner being larger than those on the inner side. This feature of our solution agrees with the earlier detailed numerical simulations of Ref. 7, see Fig. 9 a of that paper.

The velocity perturbations during the developed stage of the instability are related to each other by equations that follow from Eqs (58), (59) and (63):

$$\dot{f}_\varphi = \frac{m}{\left(m^2 + k^2 a_0^2\right)\kappa_1}\dot{f}_r; \quad \dot{f}_z = -\frac{k a_0^2}{\left(m^2 + k^2 a_0^2\right)\kappa_1}\dot{f}_r. \tag{64}$$

The random, not deliberately machined, perturbations are also dominated by the mass-density perturbations that contain the additional large parameter of the inverse shell thickness compared to the surface waviness. Initially present imperfections in the structure of the material also contribute mostly to the density perturbations. So, Eqs. (62) are relevant for this case as well.

D. Initial value problem for the parabolic *g(t)*

In this section we analyze in more detail a particular, parabolic, shape of the *g(t)* function at an early stage of the implosion, Eq. (7). For the parabolic model, the shell

radius changes according to Eq. (8). We consider the times $t \le \tau$, for which the shell radius can be considered as constant, whereas the growth of the perturbations can be significant,

Our governing equation (50) can then be rewritten as:

$$\frac{d^2 f_r}{d\tilde{t}^2} = S_{1,2}\tilde{t}^2 f_r , \tag{65}$$

where

$$\hat{t} = \frac{t}{\tau}, \;\; S_{1,2} = 2\left(m^2 + k^2 a_0^2\right)\frac{\kappa_{1,2}}{a_0} = -Qa_0 \pm \sqrt{\left(Qa_0\right)^2 + 4\left(m^2 + k^2 a_0^2\right)} . \tag{66}$$

The dimensionless parameter S_1 is positive, whereas S_2 is negative. The basis functions $Y_{1,2}$, $Z_{1,2}$ are presented in Appendix B.

Consider this solution for the case of machined perturbations of Sec. C. In this case the surface ripple f_r is determined by the first of Eqs. (55) . We have:

$$\frac{f_r}{a_0} = \frac{\xi}{2h} \times \frac{Y_1\left(S_1^{1/4}\hat{t}\right) - Y_2\left(\left|S_2\right|^{1/4}\hat{t}\right)}{\sqrt{\left(Qa_0\right)^2 + 4\left(m^2 + k^2 a_0^2\right)}} \tag{67}$$

and

$$\frac{f_\mu}{\mu_0} = \frac{\xi}{4h} \times \frac{-S_2 Y_1\left(S_1^{1/4}\hat{t}\right) + S_1 Y_2\left(\left|S_2\right|^{1/4}\hat{t}\right)}{\sqrt{\left(Qa_0\right)^2 + 4\left(m^2 + k^2 a_0^2\right)}} \tag{68}$$

As a measure of the perturbation growth at this stage we use the ratio $f_\mu(\hat{t}=1)/f_{\mu 0}$:

$$H_1 \equiv \frac{f_\mu\left(t=\tau\right)}{f_{\mu 0}} = \frac{-S_2 Y_1\left(S_1^{1/4}\right) + S_1 Y_2\left(\left|S_2\right|^{1/4}\right)}{-S_2 + S_1} \tag{69}$$

As an illustration, we plot this ratio as a finction of the wave number for the case of axisymmetric perturbations (m=0) with B_z=0 (Fig. 5). One sees that the growth is modest, even for ka=10. Given the low acceleration at the beginning of the implosion ($g \sim t^2$), this is not surprising. Contributing to this modest growth is also the absence of initial velocity: the machined perturbations start growing from the zero-velocity state. and even if the first, exponentially growing term takes over, there still remains a factor $\left|S_2\right|/\left(\left|S_2\right|+S_1\right) < 1$ in font of it. Thus factor holds a memory of the initial condition.

We emphasize that this stage cannot be described in terms of an instantaneous growth factor, due to the violation of the applicability conditions of the WKB approximation early in the pulse. In the model of the instantaneous growth rate the perturbation growth towards the end of the latent phase is simply

$$H_2 = \exp\left(\int_0^\tau \Gamma\, dt\right) = \exp\left(\sqrt{S_1}/2\right) \tag{70}$$

As an illustration, we compare this function with that of Eq. (69) or axisymmetric perturbations (m=0). Note that the function (70) has been multiplied by a factor of 0.2 in order to fit the same plot as the other curves in Fig. 5. One sees a significant difference between the function H_2 of Eq.(70) and function H_1 of Eq. (69). This indicates the need to properly account for the slow part of the growth (at early times) and for the correct

accounting for the initial conditions. The procedure that would allow one to correctly match the exact solution early in the pulse with the WKB solution at the later stage and is described in Sec. V.

Despite the modest perturbation growth, the first stage is important in that it gradually transitions to the WKB stage, eventually selecting only the growing mode with a correct amplitude determined by the initial conditions. The transition to this regime of an exponential growth means that the ratio f_r/f_μ becomes constant determined by Eq. (63). In other words, the transition occurs when the function

$$H_3 \equiv \frac{f_r\left(\hat{t}=1\right)}{\kappa_1 f_\mu\left(\hat{t}=1\right)/\mu_0} = \frac{Y_1(S_1^{1/4}) - Y_2(|S_2|^{1/4})}{Y_1(S_1^{1/4}) + (S_1/|S_2|)Y_2(|S_2|^{1/4})} \tag{71}$$

becomes close to 1 (in other words, the non-exponential term becomes negligible) at large-enough k's .The plot of this function is presented in Fig. 5 (magenta curve). One sees that the transition occurs at ka>10, when the parameter S_1 exceeds, roughly, 10. For smaller ka, in order to match the exact solution and the WKB solution, one has to follow an exact solution into domain $t>\tau$.

Now we proceed to the analysis of the growth of helical perturbations during the latent phase. This can be done based on Eq. (62) and is illustrated by Fig. 6, where the parameter S_1 is shown as a function of ka_0 for several values of m and B_z/B_φ. One can clearly see several trends. First, the axisymmetric, m=0, perturbations (Fig. 6a) grow slower for finite axial field compared to the case of no field (red curve). Second, perturbations with finite m grow faster in the presence of the axial field than in the absence of it (Fig. 6, b,c). The growth rate becomes somewhat higher than the growth-rate of m=0 perturbations in the absence of the axial field. This happens over a wide range of ka and does not require fulfillment of the resonant condition $ka = mB_\varphi/B_z$ Third, the perturbations with a "wrong" chirality (m<0) shown with the dashed curves are distinctly slower than the perturbations with a "correct" chirality (m>0). Again, this happens in a broad range of k, irrespectively to whether the resonant condition is satisfied or not.

For larger k's the parameter S_1 exceeds the values ~ 10-15 needed for the transition to a WKB regime during the latent stage. For smaller k this transition, however, does not happen and, in order to correctly relate the amplitude of the perturbation to the initial conditions, one has to solve a full-blown set of equations (44)-(46). On the other hand, this longer-wavelength perturbations grow slower, anyway, and probably have a weaker effect.

V. REGIME OF FAST PERTURBATION GROWTH

A. WKB equations

The regime that we consider now is that where condition (38) is satisfied. It can be overlapping with the end of the first phase. In the assessing of the WKB approximation it is convenient to reduce the set of equations (26)-(29) to a single equation for f_r. Eliminating f_μ from Eqs. (26) and (27) and using Eq. (30), one obtains:

$$\frac{1}{g}\frac{d^2 f_r}{dt^2} = mf_\varphi - kf_z - Qf_r\,. \tag{72}$$

The quantities f_φ and f_r are related by the vorticity equation (18). As we consider perturbations with the zero initial velocities, one has

$$ka^2 \dot{f}_\varphi + m\dot{f}_z = 0 . \tag{73}$$

One can also note that this relation will approximately hold at the developed stage of the instability even if the initial velocity perturbations were non-zero. Therefore, taking the first derivative of Eq. (72) and eliminating f_φ by Eq. (73), one finds:

$$\frac{ka^2}{m^2 + k^2 a^2} \frac{d}{dt}\left(\frac{1}{g} \frac{d^2 f_r}{dt^2} + Q f_r \right) = -\dot{f}_z \tag{74}$$

Taking one more derivative and using Eq. (29), one finds a single equation for f_r:

$$\frac{d}{dt}\left[\frac{a^2}{m^2 + k^2 a^2} \frac{d}{dt}\left(\frac{1}{g} \frac{d^2 f_r}{dt^2} + Q f_r \right) \right] = g f_r \tag{75}$$

Now we proceed to the derivation of the WKB equations. We seek a solution of this equation (75) in the form

$$f_r = e^E \tag{76}$$

where E is the eikonal. The instantaneous growth rate is

$$\Gamma = \dot{E} \tag{77}$$

so that Eq. (39) acquires the form:

$$\ddot{E} = \varepsilon \dot{E}^2 \tag{78}$$

The slowness of variation of the growth rate Γ determined by Eq. (34) means that the parameters g, a and Q that determine the growth rate are varying slowly:

$$\left| \dot{g} / g \right| \sim \varepsilon\Gamma; \ \left| \dot{a} / a \right| \sim \varepsilon\Gamma; \ \left| \dot{Q} / Q \right| \sim \varepsilon\Gamma. \tag{79}$$

Following the standard WKB approach [2], we present $\dot{E}$ as

$$\dot{E} = \dot{E}_0 + \dot{E}_1 + ... \tag{80}$$

where $\dot{E}_0$ is simply an instantaneous growth rate, Eq. (25), whereas $\dot{E}_1$ is a correction of order ε.

B. Zeroth-order WKB and exponentiation factors

As mentioned in Sec. III, the stage of the fast perturbation growth corresponds to an almost constant axial current and the scaling $g \approx g_0 (a_0 / a)$. The axial drive magnetic field at this stage is insignificant (see Sec. III), and

$$Q = \frac{2}{a}\left(\frac{m^2}{\sqrt{m^2 + k^2 a^2}} - 1 \right) , \tag{81}$$

so that

$$\Gamma = \sqrt{\frac{g}{a}} \sqrt{\left(1 - \frac{m^2}{\sqrt{m^2 + k^2 a^2}} \right) + \sqrt{\left(1 - \frac{m^2}{\sqrt{m^2 + k^2 a^2}} \right)^2 + m^2 + k^2 a^2}} \tag{82}$$

Note that, as g varies as $1/a$, the growth rate for given values of m and k depends only on a. Using this circumstance, one can present the growth factor during the phase 2 as

$$E_0 = \int_{\tau}^{t} \Gamma\, dt' = \int_{a}^{a_0} \frac{\Gamma(a)da}{|\dot{a}|} = \int_{a}^{a_0} \frac{\Gamma(a)da}{v_0\sqrt{1+9\ln(a_0/a)}}\ , \tag{83}$$

where we used Eq. (12) for the liner velocity. Using Eqs. (81)-(82) , one can represent E_0 as a function of the dimensionless wave number ka_0, m, and instantaneous radial convergence C:

$$E_0 = E_0\left(ka_0, m, C\right);\ C \equiv a_0 / a \tag{84}$$

The evolution of the perturbation in this approximation is described as e^{E_0}.

We will not write relatively lengthy intermediate equations and present only the resulting graphs of E_0 vs. C for several values of ka_0 and m (Fig. 7). One sees that indeed for a broad range of parameters, the rapid increase of the growth factor is followed by the stage of a very slow growth, as mentioned in Sec. III. Note, however, that even a further "ballistic" (non-exponential) growth of perturbations may cause significant deformation of the liner at the late stage of the implosion. This issue will be considered in Sec. VI.

C. First-order correction and a pre-exponential factor

Consider now a first-order correction. The smallness of this correction means that $E_1 << E_0$ but not necessarily that $E_1 << 1$ [24]. Accounting for this correction leads to an appearance of significant pre-exponential factors in the expression $f_r = const \times e^{E_0}$. On the other hand, the second-order correction is indeed smaller than unity [24] and is therefore of less interest. We will consistently neglect second-order terms when performing differentiations in Eq. (75), whereas the zeroth and first order terms will be retained. The corresponding calculations are presented in Appendix C. Here we discuss two particular examples.

First we consider axisymmetric, short-wavelength perturbations, $k >> a$, $m=0$. In this case q (defined by Eq. (37)) is constant, $q=k$. For $k >> a$ the growth-rate is simply $\Gamma = \sqrt{kg}$. We also note that $|Q| << k$. With these observations, we obtain from Eq. (C11):

$$\dot{E}_1 = -\frac{\dot{g}}{2g} \tag{85}$$

or

$$e^{E_0 + E_1} = \frac{const}{\sqrt{g}} e^{\int \Gamma dt} \tag{86}$$

As at the second stage of the implosion $g \sim 1/a$, the pre-exponential factor is decreasing as a square root of the convergence, thereby somewhat reducing the amplitude of the perturbations.

The second example is concerned with a short-wavelength flute mode, $k=0$, $m >> 1$. In this case

$$q^2 = \frac{m^2}{a^2};\ Qg = 2\frac{|m|g}{a};\ \Gamma^2 = \frac{|m|g}{a}\left(\sqrt{2}-1\right). \tag{87}$$

Noting that $g \sim 1/a$, one gets from Eq. (C.11):

$$\dot{E}_1 = -\frac{3\left(2-\sqrt{2}\right)\dot{g}}{8g} \tag{88}$$

so that the pre-exponent scales as approximately $(1/C)^{0.23}$. It is substantial to correctly account for for the angular momentum conservation in order to find the exponent 0.23 in this dependence.

VI BALLISTIC PERTURBATION GROWTH

A. Transition to the third stage of the implosion

In the discussion of Sec. III and V we arrived at a paradoxical conclusion that the perturbations stop growing exponentially by the end of the second stage. More accurately, the perturbation e-folding time $1/\Gamma$ becomes longer than the characteristic implosion time t^*, Eq. (13). This is a feature of the Z-pinch, with its unique relation between the drive pressure and the pinch radius (at the stage of an almost constant current). The implosion, in some sense, remains smooth till the very end, with the liner just coasting to the axis at the speed acquired and perturbations imposed at the earlier stages.

The absence of the exponential growth at the late stage does not mean that the perturbations are unimportant: they just do not grow *exponentially*, but the presence of the velocity perturbations leads to the further, *ballistic*, growth of the ripples.

We again emphasize that do not consider the very late stage of the implosion, where the plasma pressure inside the liner builds up and causes deceleration of the liner. At this stage, as well as at the following rebound, the instability of the inner surface becomes dominant. This stage goes beyond our thin-shell model and is not considered here. We note, however, that perturbations of the inner surface that appeared at the earlier stage serve as a seed for this late-stage instability.

B. Liner deformations at the ballistic stage

In this section we consider an evolution of perturbations at the stage where the exponential growth becomes unimportant and one can therefore drop the terms proportional to g in the right-hand side of equations (27)-(29). The convergence at which this transition occurs depends on m and k, see Sec. VB. The set of linear equations becomes then:

$$\begin{aligned} &\ddot{f}_r = 0 \\ &d/dt\left(a^2 \dot{f}_\varphi\right) = 0 \\ &\ddot{f}_z = 0 \end{aligned} \qquad (89)$$

Note that the velocity of in-surface azimuthal flow continues to grow as $1/a$ despite the absence of the pressure drive.

Remarkably, this “coasting stage” where the role of acceleration becomes negligible, can be fully described even if the perturbations become nonlinear due to the combination of decreasing radius and rapid ballistic growth of the displacements. In particular, the radial displacement, according to the first of the equations (89), grows linearly with time.

From this point on, we drop the assumption of the smallness of the shell deformation. We describe the non-linear evolution of the shell in the Lagrangian coordinates, marking each fluid element by its initial coordinates r_0, φ_0 and z_0. We

assume that this coasting regime begins when the shell is still weakly deformed. We, however, anticipate that eventually strong deformation will appear due to further departures of the fluid elements from their initial positions, superposed on the shrinking average radius of the shell and use the exact equations (not linearized) for the dynamics of the fluid elements. In other words, we use the following set of equations:

$$r = \sqrt{\left(a^* + \mathrm{v}^* t + \dot{f}_r t \cos S_0\right)^2 + \left(a^* \dot{f}_\varphi t \sin S_0\right)^2}\ ; \tag{90}$$

$$r^2 \dot{\varphi} = a^{*2}\, \dot{f}_\varphi \sin S_0; \tag{91}$$

$$z = z_0 + \dot{f}_z t \sin S_0 \tag{92}$$

where

$$S_0 = k z_0 - m\varphi_0 \tag{93}$$

is the phase of the mode, and a^* and v* designate the radius and velocity of the shell at the moment where the coasting model becomes correct. The time t is measured from this point. The collapse of a perfectly cylindrical shell occurs at $t=t_{\mathrm{collapse}}=-a^*/\mathrm{v}^*$ (the velocity v* is negative). The quantities $\dot{f}_r$, $\dot{f}_\varphi$ and $\dot{f}_z$ describe the components of velocity perturbations of the shell elements at t=0. These perturbations have grown from some small initial values and, although are still small at t=0, but, as we show below, they become important during the further implosion. Substituting r from Eq. (90) to Eq. (91) and performing integration, one finds:

$$\varphi = \varphi_0 + \frac{a^* \dot{f}_\varphi t \sin S_0}{a^* + \mathrm{v}^* t + \dot{f}_r t \cos S_0}. \tag{94}$$

As can be seen from the subsequent results, the last term under the square root in Eq. (90) is small and we have neglected it in Eq. (94). In the subsequent equations we also use this simplified form of Eq. (90):

$$r = a^* + \mathrm{v}^* t + \dot{f}_r t \cos S_0. \tag{95}$$

It is easy to account for the presence of initial non-zero deviations from the purely cylindrical shape at t=0. (i.e. the finiteness of f_r, f_φ, f_z. However, as they are small, their role will be insignificant compared to the accumulated effect caused by the presence of velocity perturbations, which cause the growth of deformations with time. So, we stick to the mapping defined by Eqs. (92), (94) and (95).

In the further discussion, we normalize r to a^*, z to $1/k$, and t to $t_{collapse}$, leaving φ unchanged:

$$\hat{r} = r / a^*;\ \ \hat{\varphi} = \varphi;\ \ \hat{z} = kz;\ \ \hat{t} = t\,|\,\mathrm{v}^*\,|\,/a \tag{96}$$

With that, the mapping acquires the form:

$$\hat{r} = 1 - \hat{t} + w_r \hat{t} \cos S_0;$$

$$\hat{\varphi} = \hat{\varphi}_0 + \frac{w_\varphi \hat{t} \sin S_0}{1 - \hat{t} + w_r \hat{t} \cos S_0}; \tag{97}$$

$$\hat{z} = \hat{z}_0 + \dot{f}_z \hat{t} \sin S_0,$$

where

$$w_r = \frac{\dot{f}_r}{\mathrm{v}^*};\ \ w_\varphi = \frac{\dot{f}_\varphi a^*}{\mathrm{v}^*};\ \ w_z = \frac{\dot{f}_z k a^*}{\mathrm{v}^*}. \tag{98}$$

For definiteness, we assume below that the amplitude w_r of the radial velocity perturbation is positive. One can always reach this by the appropriate shift of the phase . In other words, the perturbations with S_0=0, given the aforementioned sign convention, are lagging behind the "average" shell.

For the given values of the initial velocity perturbations (98), Eq. (97) describes a mapping of the initially cylindrical liner into a distorted one, with the shape depending on $\hat{t}$. The liner shape at a given $\hat{t}$ is characterized by the function $\hat{r}(\hat{\varphi},\hat{z},\hat{t})$ which is determined in a parametric form by Eqs. (97), with $\hat{\varphi}_0$ and $\hat{z}_0$ being parameters.

C Formation of cusps

In order for the transformation from $\hat{\varphi}_0$ and $\hat{z}_0$ to $\hat{\varphi}$ and $\hat{z}$ to be non-singular, its Jacobian must be non-zero.

$$J \equiv \frac{D(\hat{z},\hat{\varphi})}{D(\hat{z}_0,\hat{\varphi}_0)} \neq 0 \tag{98}$$

A simple calculation shows that

$$J = \frac{\left(1-\hat{t}+w_r t\cos S_0\right)^2\left(1+w_z\hat{t}\cos S_0\right) - mw_\varphi\hat{t}\left[(1-\hat{t})\cos S_0 + w_r\hat{t}\right]}{\left(1-\hat{t}+w_r\hat{t}\cos S_0\right)^2} \tag{99}$$

Initially, at small $\hat{t}$, the Jacobian is near unity, but later in time there may appear points where J becomes small or zero. One can show that this first happens near the points where S_0=0. The time when this happens should of course be less than the time when the shell implodes on the axis. These assessment depends, of course, on the velocity perturbations at $\hat{t}$ =0. The latter depend on the magnitude of the initial perturbations and cannot be predicted from the first principles. So, we will just make a scan over the amplitude of the radial perturbation, w_r. With that, one has to remember that, for a given w_r, the amplitude of the other two perturbations, w_φ and w_z are not arbitrary, as they are related to w_r by equations (64) for a=a*. We have, accordingly,

$$w_\varphi = w_r \frac{m}{\sqrt{(Qa/2)^2 + m^2 + k^2a^2} - (Qa/2)}; \tag{100}$$

$$w_z = -w_r \frac{k^2a^2}{\sqrt{(Qa/2)^2 + m^2 + k^2a^2} - (Qa/2)} \ . \tag{101}$$

We start the assessment of the formation of singularities from the simplest case of purely axisymmetric perturbations, m=0, where only Eqs. (92) and (95) are needed. In this case, the condition for the singularity formation becomes simply:

$$1 + w_z\hat{t}\cos S_0 = 0 \tag{102}$$

We see that, indeed, the singularities are first formed for S_0=0 (remember that w_z<0 for w_r>0). In other words, the singularity is formed near the area that has the strongest lag with respect to the "average" shell. The condition that the leading part of the shell (S_0=π) has not reached the axis means that (see Eq.(95)):

$$\hat{t} < \frac{1}{1+w_r} \tag{103}$$

The consistency condition (singularity is formed before a part of the shell implodes) reads then as

$$-w_z > 1 + w_r . \qquad (104)$$

Accounting for Eq. (101) and using Eq. (81) for Q, one finds that for ka>1 the singularities are formed at relatively small amplitudes of the radial velocity perturbations: w_r>0.3 for ka=2, w_r>0.28 for ka=3, and w_r>0.22 for ka=4. Fig. 8a shows the cross-section of the liner at the time when the cusps have just formed. One can check that near the cusp points, the radius changes according to equation $r_0 - r \propto |z - z_0|^{2/3}$, where the subscript "0" corresponds to the tip of the cusp. Note that the cusp points in the outward direction, this being consistent with the Ott's analysis of the planar case (Ref. 2) and detailed numerical simulations of Ref. 7 (see Fig. 9 of that paper). As was pointed out to the author by A.L. Velikovich, the idea of cusp formation in the wave motion has been described as early as 1802 [28]. This two-century old study is summarized in the Lamb's "Hydrodynamics" [29], see Sec. 251 of that book.

At later times, our mapping fails. An interesting conjecture was made in Ref. 2, where it was hypothesized that the shell material will continue flowing into the cusp leading to formation of a jet-like structure, see Fig. 4 in Ref. 2 and Fig.1 in Ref. 4. The formation of cusps seems to be identified in experiments [28-30], although for the wavelengths shorter than those covered by the thin-shell theory. Cusps may have significant effect on the efficiency of the fuel compression in fusion applications of Z-pinches. The analysis of this part of the problem goes, however, well beyond the scope of our study.

Another interesting example is that of a flute-like perturbation with k=0, $m \neq 0$. In this case one has to set w_z=0 in Eq. (98). This leads to the following equation that determines the cusp formation:

$$1 - \hat{t} + w_r \hat{t} - m w_\varphi \hat{t} = 0 \qquad (105)$$

For k=0 one has Q=$|m|$/2a, so that, according to Eq. (101), $w_\varphi = |m| w_r / \left(\sqrt{2} - 1\right)$. The time when the cusp is formed is then

$$\hat{t} = \frac{1}{1 + w_r \left(\sqrt{2} + \dfrac{|m| - 1}{\sqrt{2} - 1} \right)} \qquad (106)$$

It is universally shorter than the time (103) for the shell collapse on axis. We see that for the purely azimuthal perturbations (k=0) the cusp structures are formed more easily than for the axisymmetric modes (m=0), due to enhancement of the azimuthal velocity by virtue of the vorticity conservation. An example is shown in Fig. 8b. For the helical perurbations the cusps are formed along the line of a constant phase S_0=0. A three-dimensional rendition of this structure is shown in Fig. 9a.

The mapping (90)-(92) can be generalized to the case where perturbation is caused by multiple modes. In this case, singularities do not necessarily appear along the lines – they can be formed in the isolated points and the orientation of the cusps (inward vs. outward) becomes dependent on the amplitudes and mutual phasing of the modes. In principle, other types of singularities, in particular, folds (e.g. Ref. 31) may form. A three-dimensional image of the structure produced by the mixture of two modes is shown in Fig. 9b. We leave a general analysis of the shapes of these singularities for a future work.

VII SUMMARY AND DISCUSSION

A thin-shell model of the liner implosion is applicable to perturbations with the wave numbers smaller than the shell inverse thickness (i.e, with the wavelength longer than a few thicknesses). With this limitation, the model allows one to obtain a surprisingly complete and detailed description of the evolution of broad range of perturbations.

Within this model we identified four qualitatively different stages of the implosion: a "cold start", with the barely moving liner but perturbations already growing; the stage of a rapid acceleration and intense exponential perturbation growth; the stage of ballistic non-linear deformations and formation of singularities; the stage of stagnation and rebound (not covered by our analysis).

The first phase is interesting in that the presence of the axial driving field can be important during it, whereas at the later stages the axial field is completely overwhelmed by the orders of magnitude higher azimuthal field. At an early stage, however, the axial field can affect the onset of the helical perturbations that seed the further implosion. Another interesting feature of the first phase is a relatively slow growth of the pre-machined surface perturbations, especially if they are imposed on the outer surface only.

For the second phase, a consistent set of WKB equations has been derived. This stage (as well as the following one) is characterized by a rapid decrease of the pinch radius. Due to that, the vorticity conservation becomes important for the evolution of non-axisymmetric perturbations. We go beyond the zeroth-order of the WKB and derive the expression of the pre-exponential factor that affects significantly the perturbation amplitude at higher convergences.

Somewhat paradoxically, the exponential growth becomes less important at the later, third stage of the implosion. This happens not due to the decrease of the growth rate (that actually increases) but rather due to a shortening of the implosion time, $a/|\dot{a}|$. The absence of the exponential growth does not mean that the liner deformations stop to grow, but the growth is now mainly determined by the inertial (ballistic) motion of the elements of the shell, generated at the previous stage. By neglecting the acceleration drive, one arrives at a mapping that describes the non-linear evolution of the shell at this stage. For single-mode perturbations, the cusp structures are formed. An arbitrary mixture of the modes is also covered by this mapping.

One has to remember that all these results refer only to a thin liner model and do not cover the smaller-scale perturbations. Still, the insights developed in the present work may help one to get a broader understanding of the general picture. Also, our results can be used for interpretation of the experiments with pre-imposed perturbations.

Acknowledgment

The author is grateful to Dr. A.L. Velikovich for a valuable discussion. This work was performed under the auspices of the U.S. Department of Energy by Lawrence Livermore National Laboratory under Contract DE-AC52-07NA27344, with support from Sandia National Laboratories (Albuquerque).

Appendix A. Magnetic field perturbation at the plasma boundary

We assume vacuum outside the liner. The vacuum (curl-free) field perturbations can be presented as

$$\delta \boldsymbol{B} = -\nabla \psi \tag{A1}$$

where $\psi(r,z.\varphi,t)$ is a scalar potential. The potential ψ satisfies the Laplace equation that reads (for the perturbations harmonic in φ and z):

$$\frac{1}{r}\frac{\partial}{\partial r} r \frac{\partial \psi}{\partial r} - \left(\frac{m^2}{r^2} + k^2 \right) \psi = 0 \,. \tag{A2}$$

[More general situation where the presence of a force-free low-pressure plasma outside the liner allows for the force-free configurations has been considered in Ref. 32.]

The solution of Eq. (A2) that does not diverge at large radii is

$$\psi = C K_m(kr) \,, \tag{A3}$$

where K_m is a Hankel function of an imaginary argument. We assume that $k>0$, whereas m can be both negative and positive (and zero). The perturbation of the radial component of the magnetic field at the liner boundary is:

$$\delta B_r = -CkK'_m(ka) \,, \tag{A4}$$

where the derivative is taken over the whole argument (ka). For the harmonic perturbations the other two components (which have a cosine dependence in the notation of Eq. (24)-(25)) are:

$$\delta B_\varphi = (m/r) C K_m(kr); \delta B_z = k C K_m(kr) \,. \tag{A.5}$$

The magnetic field has to stay aligned with the perturbed surface. In the linear approximation the normal to the liner surface is $(1, \partial \xi_r / a \partial \varphi, \partial \xi_r / \partial z)$. Accordingly, the alignment condition in the linear approximation is: $\delta B_r + B_\varphi \partial \xi_r / a \partial \varphi + B_z \partial \xi_r / \partial z = 0$. This condition yields the following relation between the multiplier C in Eq. (A3) and the amplitude f_r of the radial surface displacement:

$$C = \frac{kaB_z - mB_\varphi}{kaK'_m} f_r \,. \tag{A6}$$

The magnetic pressure perturbation on the liner surface is:

$$\delta p = \frac{1}{4\pi} \left(B_\varphi \delta B_\varphi - \frac{\xi_r}{r} B_\varphi^2 + B_z \delta B_z \right), \tag{A7}$$

Here the second term accounts for the fact that the unperturbed azimuthal magnetic field varies as $1/r$ outside the liner (Cf. Ref. 16). This term is responsible for the sausage instability of an equilibrium pinch [16]. Then, using Eq. (A.5) and eliminating C by virtue of Eq. (A6) and using Eq. (A5), we find that

$$f_p = \frac{f_r}{4\pi a} \left[\left| \frac{K_m}{K'_m} \right| \frac{\left(mB_\varphi - kaB_z \right)^2}{ka} - B_\varphi^2 \right]. \tag{A8}$$

Note an error in the corresponding equation (50) of Ref. 1 where a numerical factor in front of the last term in the square bracket is ½ instead of 1. This, however, does not affect the qualitative conclusions of Ref. [1]. Returning to our Eq.(30), we find parameter Q as in Eq. (31).

Appendix B. Linearly independent solutions of Eq. (65)

We write Eq. (58) for the eigenfunctions Y in the dimensionless form:

$$\frac{d^2Y}{dx^2} = x^2 Y \tag{B1}$$

$$\frac{d^2Y}{dx^2} = -x^2 Y \tag{B2}$$

These are Weber equations whose solutions can be expressed in term of the modified Bessel functions $K_{1/3}$ [33]. For the purposes of solving the initial value problem it is, however, more convenient to choose a different set of linearly-independent functions. Specifically, we choose the first solution of Eq. (B1) as a solution which is equal to 1 at x=0 and its derivative at this point is equal to zero. This solution exponentially grows at large x and is shown by a red line in Fig. 10. The other solution, Z_1, is chosen so that it is equal to 1 at x=0 and exponentially decreases at large x. This solution is shown by a green line in Fig. 10. The derivative at x=0 is equal to - 0.7.

Consider now equation (B2). It has oscillatory solutions. As before, we choose the first one (Y_2) as equal to 1 and having a zero derivative at x=0. This solution is shown in magenta. The second solution (Z_2) is chosen to be zero at x=0 and have exactly the same derivative at x=0 as the "green" curve for Eq. (B1). A convenience of this choice becomes clear when one solves the initial value problem.

Appendix C Derivation of the pre-exponent for the WKB approximation

In deriving an expression for the first-order correction it is convenient to introduce wave number q, Eq. (37). In the derivation we will consistently neglect the terms of the second, third, etc. order in ε. This means that we retain only first derivatives of the coefficients q, g and Q that enter Eq. (75). This allows us to write Eq. (75) in an approximate form:

$$\frac{d^4 f_r}{dt^4} + Qg\frac{d^2 f_r}{dt^2} - q^2 g^2 f_r = \frac{d\left(gq^2\right)}{gq^2 dt}\frac{d^3 f_r}{dt^3} - gq^2\frac{d}{dt}\left(\frac{Q}{q^2}\right)\frac{df_r}{dt} \tag{C1}$$

where the right-hand-side is of the first order. Using the eikonal representation (76), we have, to the first order in the parameter ε:

$$\begin{aligned} &\frac{df_r}{dt} = e^E\dot{E};\ \ \frac{d^2 f_r}{dt^2} = e^E\left(\dot{E}^2 + \ddot{E}\right); \\ &\frac{d^3 f_r}{dt^3} = e^E\left(\dot{E}^3 + 3\dot{E}\ddot{E}\right);\ \ \frac{d^4 f_r}{dt^4} = e^E\left(\dot{E}^4 + 6\dot{E}^2\ddot{E}\right) \end{aligned} \tag{C2}$$

Substituting these results into Eq. (C1) and retaining only terms up to the first order (i.e., neglecting the products of $\ddot{E}$ and derivatives of the coefficients Q, g and q), we obtain:

$$\left(\dot{E}^4 + 6\dot{E}^2\ddot{E}\right) + Qg\left(\dot{E}^2 + \ddot{E}\right) - q^2 g^2 = \frac{d\left(gq^2\right)}{gq^2 dt}\dot{E}^3 - gq^2\frac{d}{dt}\left(\frac{Q}{q^2}\right)\dot{E} \tag{C3}$$

Now, we substitute $\dot{E} = \dot{E}_0 + \dot{E}_1$ and again retain only the terms to the first order (in particular, in the right-hand side we retain only terms proportional to $\dot{E}_0$). We recall also

that $\dot{E}_0 = \Gamma$, with Γ being the solution of the instantaneous dispersion relation (34). This yields:

$$\frac{\partial D}{\partial \Gamma}\dot{E}_1 + (6\Gamma^2 + Qg)\dot{\Gamma} = \frac{d\left(gq^2\right)}{gq^2 dt}\Gamma^3 - gq^2\frac{d}{dt}\left(\frac{Q}{q^2}\right)\Gamma \tag{C4}$$

The temporal variation of the instantaneous growth rate, $\dot{\Gamma}$, is caused by the variation of the coefficients in the instantaneous dispersion relation (34) and can be found by differentiating it over the time. This procedure yields:

$$\dot{\Gamma} = \frac{\dfrac{d\left(q^2g^2\right)}{dt} - \Gamma^2\dfrac{d(Qg)}{dt}}{2\Gamma\left(2\Gamma^2 + Qg\right)} \tag{C5}$$

Substituting this into Eq. (C4) we find:

$$\Gamma\frac{\partial D}{\partial \Gamma}\dot{E}_1 = \frac{d\left(gq^2\right)}{gq^2 dt}\Gamma^4 - gq^2\frac{d}{dt}\left(\frac{Q}{q^2}\right)\Gamma^2 - \left(6\Gamma^2 + Qg\right)\frac{\dfrac{d\left(g^2q^2\right)}{dt} - \Gamma^2\dfrac{d(Qg)}{dt}}{2\left(2\Gamma^2 + Qg\right)} \tag{C6}$$

We will now repeatedly use an equation that is equivalent to Eq. (34),

$$\Gamma^4 = q^2g^2 - Qg\Gamma^2 \tag{C7}$$

both in the left-hand side and the right-hand side. In particular, we have

$$\Gamma\frac{\partial D}{\partial \Gamma} = 2\left(2q^2g^2 - Qg\Gamma^2\right). \tag{C8}$$

After rather lengthy calculations, we arrive at the following relatively compact expression:

$$\dot{E}_1 = \frac{-\Gamma^2\left(\dfrac{2}{g^2}\dfrac{d\left(q^2g^4\right)}{dt} + \dfrac{3}{2}\dfrac{d(Qg)^2}{dt}\right) + \dfrac{g^2}{Qg}\dfrac{d\left[q(Qg)\right]^2}{dt}}{4\left(2\Gamma^2 + Qg\right)\left(2q^2g^2 - Qg\Gamma^2\right)} \tag{C9}$$

where Γ^2 is a positive root of Eq. (34). One may also find helpful an easily verifiable identity

$$\left(2\Gamma^2 + Qg\right)\left(2q^2g^2 - Qg\Gamma^2\right) = g^2\left(Q^2 + 4q^2\right)\Gamma^2 \tag{C10}$$

that leads to a somewhat more compact expression for $\dot{E}_1$:

$$\dot{E}_1 = \frac{-\left(\dfrac{2}{g^2}\dfrac{d\left(q^2g^4\right)}{dt} + \dfrac{3}{2}\dfrac{d(Qg)^2}{dt}\right) + \dfrac{g^2}{Qg\Gamma^2}\dfrac{d\left[q(Qg)\right]^2}{dt}}{4g^2\left(Q^2 + 4q^2\right)} \tag{C11}$$

References

1. E. G. Harris. “Rayleigh-Taylor Instabilities of a Collapsing Cylindrical Shell in a Magnetic Field.” Phys. Fluids, **5**, 1057 (1962).
2. E. Ott. “Nonlinear Evolution of the Rayleigh-Taylor Instability of a Thin Layer.” Phys. Rev. Lett. **29**, 1429 (1972).
3. Yu.A. Bashilov, S.V. Pokrovskii. “Nonlinear Evolution of Rayleigh-Taylor Instability in a Thin Cylindrical Shell.” Sov. Phys. Tech. Phys. **22**, 1306 (1977).
4. M.M. Basko, Rayleigh-Taylor eigenmodes of a thin layer in the nonlinear regime”, Phys. Plasmas, **1**, 1270 (1994).
5. D.D. Ryutov, M.S. Derzon, M.K. Matzen. “The physics of fast Z pinches.” Rev. Mod. Phys., **72**, 167 (2000).
6. M. G. Haines. “A review of dense Z-pinches.” Plasma Phys. Controlled Fusion, **53**, 093001 (2011).
7. S. A. Slutz, M. C. Herrmann, R. A. Vesey, A. B. Sefkow, D. B. Sinars, D. C. Rovang K. J. Peterson, and M. E. Cuneo. “Pulsed-power-driven cylindrical liner implosions of laser preheated fuel magnetized with an axial field.” Phys. Plasmas, **17**, 056303 (2010).
8. Stephen A. Slutz and Roger A. Vesey. “High-Gain Magnetized Inertial Fusion,” Phys. Rev. Lett., **108**, 025003 (2012).
9. M.R. Gomez et al. “Experimental demonstration of fusion-relevant conditions in magnetized liner inertial fusion.”Phys.Rev.Lett., accepted, August 2014.
10. M.K. Matzen, “Z pinches as intense x-ray sources for high-energy density physics applications.” Phys. Plasmas, **4**, 1519 (1997).
11. M.E. Cuneo, Waisman, EM; Lebedev, SV Chittenden, JP; Stygar, WA Vesey, et al. “Characteristics and scaling of tungsten-wire-array z-pinch implosion dynamics at 20 MA” Phys. Rev. E, **71**, 046406 (2005).
12. S.V. Lebedev, D.J. Ampleford, A. Ciardi, S.N. Bland, J.P. Chittenden, M.G. Haines, A. Frank, E.G. Blackman, A. Cunningham. Astrophys. J., **616**, 988 (2004).
13. B.A. Remington, R.P. Drake, D.D. Ryutov, "Experimental astrophysics with high-power lasers and Z pinches", Rev. Mod. Phys., **78,** 755 (2006).
14. M. D. Kruskal, J. L. Johnson, M. B. Gottlieb, and L. M. Goldman. “Hydromagnetic instability in a stellarator.” Phys. Fluids **1**, 421 (1958).
15. V. D. Shafranov, “The stability of a cylindrical gaseous conductor in a magneyic field.” Soviet Atomic Energy, v.1, p. 709, 1956; translated from Atomnaya Energiya,” **5**, 38 (1956).
16. B. B. Kadomtsev, *Reviews of Plasma Physics*, edited by M. A. Leontovich (Consultants Bureau, New York, 1966), Vol. 2, p. 153.
17. M.A. Raadu. “Suppression of kink instability for magnetic flux ropes in chromosphere.” Solar Phys., **22**, 425 (1972).
18. D.D. Ryutov, I. Furno, T.P. Intrator, S. Abbate, T. Madziwa-Nussinov. "Phenomenological theory of the kink instability in a slender plasma column", Phys. Plasmas, **13,** 032105, (2006).
19. G.L. Delzanno, E.G. Evstatiev, J.M. Finn. “Line-tied kink modes in cylindrical equilibria with magnetic shear.” Phys. Plasmas, **14**, 072902, 2007.

20. T.P. Intrator, X. Sun, L. Dorf, J.A. Sears, Y. Feng, T.E. Weber, H. O. Swan. Flux ropes and 3D dynamics in the relaxation scaling experiment," Plasma Phys. Contr. Fus., **55**, 124005 (2013).
21. T. J. Awe, R. D. McBride, C. A. Jennings, D. C. Lamppa, M. R. Martin, D. C. Rovang, S. A. Slutz, M. E. Cuneo, A. C. Owen, D. B. Sinars, K. Tomlinson, M. R. Gomez, S. B. Hansen, M. C. Herrmann, J. L. McKenney, C. Nakhleh, G. K. Robertson, G. A. Rochau, M. E. Savage, D. G. Schroen, and W. A. Stygar. "Observations of Modified Three-Dimensional Instability Structure for Imploding **z**-Pinch Liners that are Premagnetized with an Axial Field." Phys. Rev. Lett., **111**, 235005 (2013).
22. T. J. Awe, C. A. Jennings, R. D. McBride, M. E. Cuneo, D.C. Lamppa, M. R. Martin, D. C. Rovang, D. B. Sinars, S. A. Slutz, A. C. Owen, K. Tomlinson, M.R. Gomez, S. B. Hansen, M. C. Herrmann, M.C. Jones, J. L. McKenney, G. K. Robertson, G. A. Rochau, M. E. Savage, D. G. Schroen, and W. A. Stygar. "Modified helix-like instability structure on imploding z-pinch liners that are pre-imposed with a uniform axial magnetic field." Phys. Plas. **21**, 056303 (2014).
23. S.A. Slutz, M.R. Douglas, J.S. Lash, R.A. Vesey, G.A. Chandler, T.J. Nash, M.S. Derzon. "Scaling and optimization of the radiation temperature in dynamic hohlraums." Phys. Plasmas, **8**, 1673 (2001).
24. L.D. Landau and E.M. Lifshitz. *Quantum Mechanics, Nonrelativistic Theory*. Pergamon, NY 1977.
25. D.D. Ryutov. "Liner-on-plasma system: Stabilizing effect of a magnetic cushion near the stagnation point," Phys. Plasmas, **18**, 064509 (2011).
26. F. Gerstner. "Theorie der Wellen." Abhandlungen der Königl. Bömischen Gesellshaft der Wissenschaftenzu Prag für das Jahr 1802 (in German), p. 412 (1802)
27. H. Lamb. *Hydrodynamics*. Dover Publications, NY, 1945.
28. D.B. Sinars, S.A. Slutz, M.C. Herrmann et al. "Measurements of Magneto-Rayleigh-Taylor Instability Growth during the Implosion of Initially Solid Al Tubes Driven by the 20-MA, 100-ns Z Facility." Phys. Rev. Lett., **105**, 185001 (2010).
29. D.B. Sinars, S.A. Slutz, M.C. Herrmann et al. "Measurements of magneto-Rayleigh-Taylor instability growth during the implosion of initially solid metal liners." Phys. Plasmas, **18**, 056301 (2011).
30. R. McBride, M. R. Martin , R. W. Lemke , J. B. Greenly , C. A Jennings , D. C. Rovang , D. B. Sinars , M. E. Cuneo , M. C. Herrmann , S. A. Slutz , C. Nackleh , D. D. Ryutov , J-P. Davis , D.G. Flicker , B. E. Blue , Kurt Tomlinson , D.G. Schroen , R. Stamm , G. Smith , J. Moore , T. Rogers , G. Robertson , R. Kamm , I. Smith , M. Savage , W. A. Stygar , G.A. Rochau , M.l. Jones, M. Lopez , J. L. Porter , M. K. Matzen. "Beryllium liner implosion experiments on the Z accelerator in preparation for Magnetized Liner Inertial Fusion (MagLIF)." Phys. Plasmas, **20**, 056309 (2013).
31. V.I. Arnold. *Catastrophe Theory*, 3rd ed. Berlin: Springer-Verlag, 1992.
32. D.D. Ryutov T.J. Awe, S. Hansen, H R. McBride, K.J. Peterson, D.B. Sinars, S.A. Slutz. "Effect of Axial Magnetic Flux Compression on the Helical Mode of the Magnetic Rayleigh-Taylor Instability (Theory)." Paper presented at 9th International Conference on Dense Z-Pinches (DZP 2014).
33. H. Bateman, A. Erdelyi. "*Higher Transcendental Functions*," v. 2, Mc Graw-Hill Book Company, New York, Toronto, London (1953).

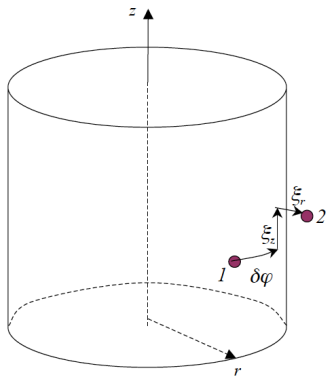

Fig. 1 Displacement of a fluid element with respect to its initial position "1" on the unperturbed liner to position "2" corresponding to perturbed liner. If the liner performs un-perturbed motion, both $\xi_r, \delta\varphi$ and ξ_z are zero. When perturbation is present, the magnitudes of these three displacements are measured from the point 1 on the unperturbed imploding liner, i.e., point 1 is moving.

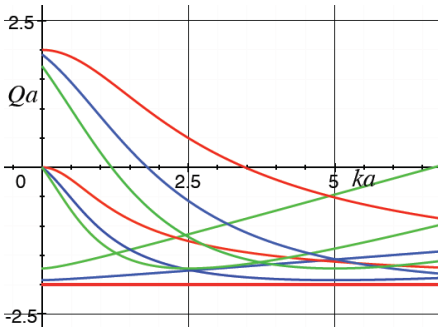

Fig. 2 The parameter Q vs the dimensionless wave number, ka, for several values of the ratio of B_z/B_τ: 0 (red lines), 0.2 (blue lines) and 0.4 (green lines). The curves in each group of the same color correspond to m=0, 1 and 2 from the bottom to the top.

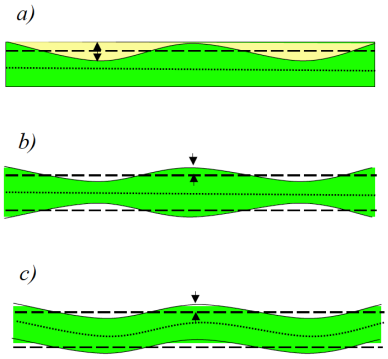

Fig. 3. On the relation between the surface mass density perturbation $f_{\mu 0}$ and the initial displacement f_{r0} for the machined liner: *a*) A liner (green) of thickness h with sinusoidal perturbation produced by removing material from the outer surface. The removed material is shown in yellow; ζ is the maximum thickness of the material removed (we consider ζ as a positive quantity). In the linear approximation ζ is assumed to be small compared to the shell thickness, h. In the figure this thickness is exaggerated for the better visibility. The average unperturbed surface (dashed line) is situated at the distance $\zeta/2$ from the initial surface. Dotted line represents a median surface. This perturbation can be decomposed into a symmetric

one, *b*), that represents the mass-density perturbation, and an asymmetric one, *c*), that represents the bending of the liner. Superposing *b*) and *c*) one would get a shape shown in *a*).

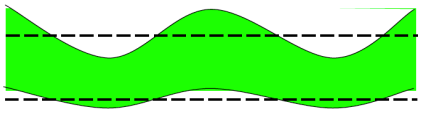

Fig. 4. At the developed (but still linear) stage, ripples on the outer side (upper surface in this figure) of the shell remain larger than on the inner side (lower surface on this figure).

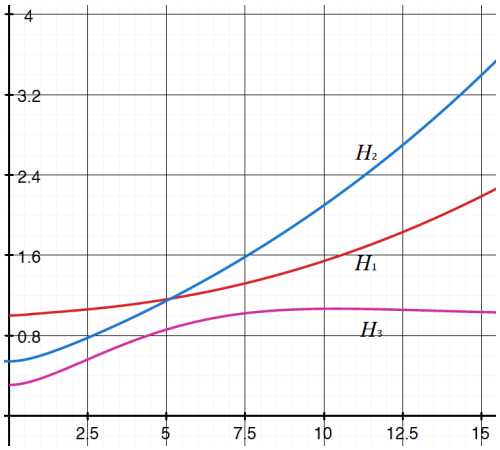

Fig. 5 The function H_1 (Eq. (69)) characterizing the perturbation growth by the end of the latent phase *vs*. *ak* (red curve). The blue curve shows the function H_2 (Eq. (70)) characterizing the perturbation growth in the model of the instantaneous growth rate. To fit the same plot, the function H_2 is multiplied by 0.2. Magenta curve (Eq. (71)) characterizes the transition of the exact solution (Eq. (62)) to the developed stage, where the WKB approximation becomes applicable. The transition occurs at ka~7-10.

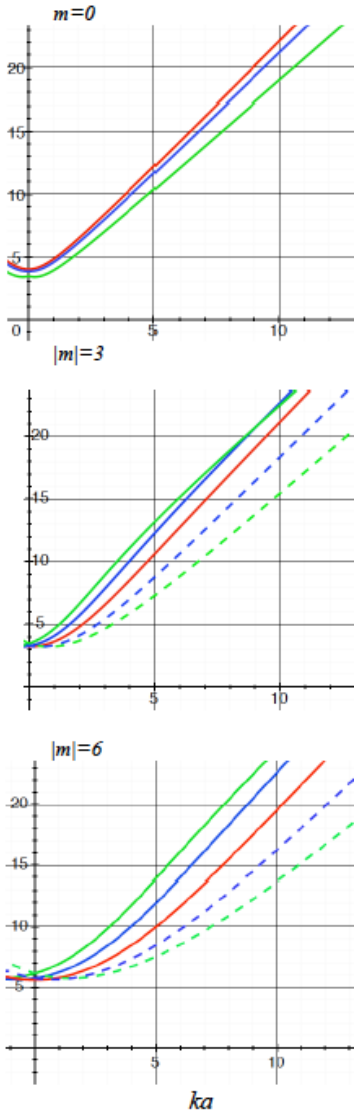

Fig. 6. The parameter S_1 characterizing the perturbation growth during the latent phase (Eqs. (65), (66)) vs. ka. Red curves correspond to $B_z=0$, blue curves correspond to $B_z=0.2B_*$, and green curves correspond to $B_z=0.4B_*$. Solid lines correspond to positive m, whereas dashed lines correspond to negative m (i.e. to the chirality of the perturbations opposite to that of the magnetic field lines).

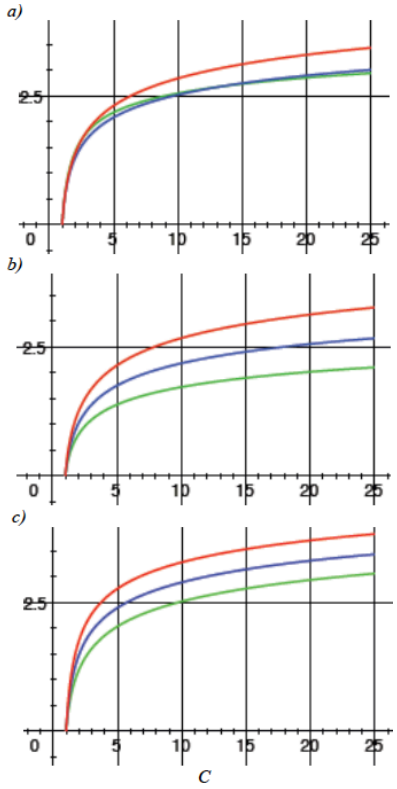

Fig. 7. WKB growth factor G vs. convergence C: a) m=3 for all curves, ka=1 (green); ka=3 (blue); ka=5 (red); b) ka=0 for all curves; m=1 (red curve); m=3 (blue curve); m=5 (green curve); c) m=0 for all curves, ka=1 (green); ka=3 (blue) ka=5 (red)

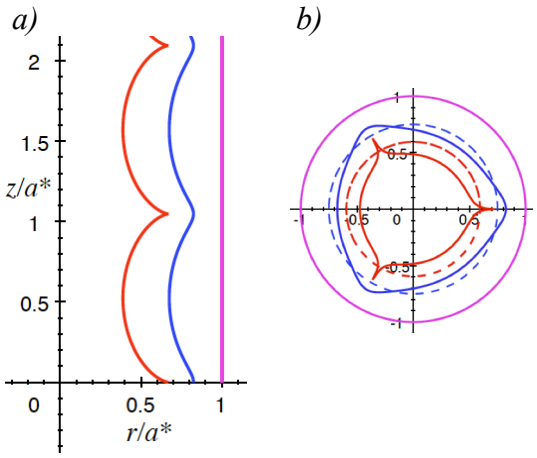

Fig. 8 Cusp formation in the imploding liner: a) Vertical cross-section showing evolution of the axisymmetric mode with m=0, ka*=6. All the dimensions are normalized to a*. The initial position is shown in magenta, the intermediate position is shown in blue; the instant of the cusp formation is sown in red. Initial amplitude of the radial velocity perturbation is 0.3v*. b) Horizontal cross-section showing he evolution of the z-independent mode, k=0, m=3. The color coding is the same as in the left panel. Dashed lines show the unperturbed liner positions at the same instants of time as the solid curves. Initial amplitude of the radial velocity perturbation is 0.2v*.

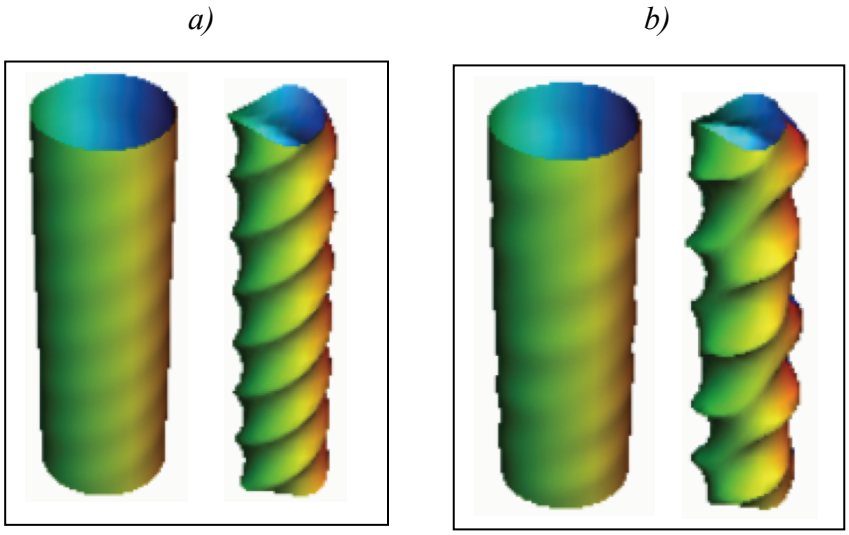

Fig. 9. Three-dimensional images showing nonlinear evolution of the liner. a) The helical mode with ka=7, m=3, halfway to the cusp formation and at the time when cusps are formed. b) The same image for the case where two modes are present: an axisymmetric mode with ka=5, m=0, and the helical mode with ka=7, m=3. Initial radial velocity perturbations for the modes are 0.2v*.

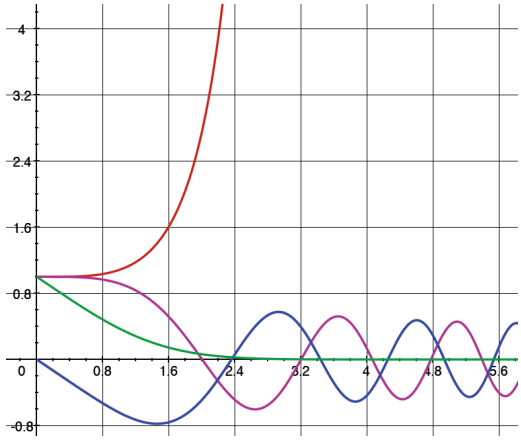

Fig. 10. Eigenfunctions for Eqs. (B1) and (B2): Y_1 (red); Y_2 (green); Z_1 (magenta); Z_2 (blue).